JACS
JOURNAL OF THE AMERICAN CHEMICAL SOCIETY
Article
pubs.acs.org/JACS

Binding and Packing in Two-Component Colloidal Quantum Dot Ligand Shells: Linear versus Branched Carboxylates

Kim De Nolf,[†,‡] Salvatore M. Cosseddu,[¶] Jacek J. Jasieniak,[§] Emile Drijvers,[†,‡] José C. Martins,[∥] Ivan Infante,[¶] and Zeger Hens*[,†,‡]

[†]Physics and Chemistry of Nanostructures, [‡]Center for Nano and Biophotonics, and [∥]NMR and Structural Analysis Unit, Ghent University, 9000 Gent, Belgium

[¶]Department of Theoretical Chemistry, Vrije Universiteit, 1081 HV AmsterdamNetherlands

[§]ARC Centre of Excellence in Exciton Science, and Department of Materials Science and Engineering, Monash University, Clayton, Victoria 3800, Australia

Supporting Information

ABSTRACT: In this work, we present a combined experimental and theoretical analysis of two-component ligand shells passivating CdSe quantum dots. Using nuclear magnetic resonance spectroscopy, we first show that exposing oleate-capped quantum dots to primary carboxylic acids results in a one-for-one exchange that preserves the overall ligand surface concentration. Exposure to straight-chain acids leads to a binary ligand shell that behaves as an ideal mixture and that has a composition matching the overall acid composition of the dispersion. In the case of branched-chain acids, the exchange is restricted to about 25% of the original ligands. Based on molecular dynamics simulations, we argue that this behavior reflects the more favorable packing of oleates compared to branched carboxylates on the (100) facets of CdSe quantum dots.

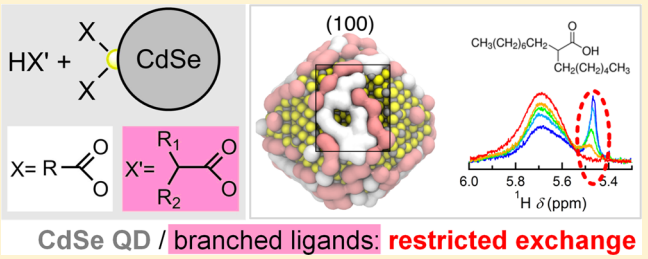

INTRODUCTION

Colloidal nanocrystals (NCs) are hybrid organic/inorganic nano-objects composed of a nanometer-sized inorganic core that is terminated by an organic capping or ligand shell.[1,2] Typical ligands, such as carboxylic acids, thiols, amines, or phosphonic acids, feature a functional headgroup that adheres to the NC surface and a hydrocarbon chain that provides steric stabilization in the reaction mixture and purified NC dispersions. Ligand type, concentration, and chain length have proven to be highly useful reaction variables for tuning the NC size[3,4] and shape[5,6] during synthesis. Furthermore, tightly bound ligands enable NC powders to be readily redispersed in appropriate solvents without aggregration.[7] This practical advantage has facilitated the ongoing proliferation of colloidal NCs in a diverse range of applications, including lighting and displays,[8] photovoltaics,[9] photodetection,[10] sensing,[11] and catalysis.[12]

For most NC applications, a suitable surface passivation has proven essential to achieve optimized processing and device performance metrics. Gold NCs, for example, have been turned into colorimetric sensors when functionalized with ligands that expose chelating groups to the surroundings which coordinate specific analytes to cause an aggregation-induced color change.[11] In the case of semiconductor NCs or quantum dots (QDs), the replacement of the typically used long alkyl chained aliphatic ligands by small organic or inorganic moieties has led to QD films with high electrical mobilities[13] and has provided tunability of the QD workfunction.[14] Such aspects are now being widely explored in QD nanoelectronics,[15] photodetectors,[16] and solar cells.[17] In addition, numerous studies have addressed the relationship between the ligand surface coverage and the photoluminescence quantum yield of QDs,[18−20] which is essential for the application of QDs in lighting, displays, and solar concentrators.

The adsorption of ligands onto the nanocrystals surface has been traditionally compared to the formation of self-assembled monolayers (SAMs) on flat surfaces. Alkanethiols on gold stand out as one of the most-studied SAM model systems, as well as being a widely used colloidal NC/ligand combination.[21−23] SAMs organize on solid surfaces through a combination of headgroup−substrate and chain−chain interactions. The aforementioned examples highlight that in the case of colloidal NCs, ligand binding is mainly addressed from the perspective of headgroup−substrate interactions. However, in the case of two-component SAMs that contain molecules with identical headgroups, but slightly dissimilar chains, chain−chain interactions can cause phase separation into nanometer scale, molecular domains;[24] a size commensurate with that of a NC surface facet. Given the similarity between SAMs and ligand shells, such a finding suggests that chain−chain interactions may also determine the packing of ligands on NC surfaces.

Received: October 31, 2016
Published: February 13, 2017

DOI: 10.1021/jacs.6b11328
J. Am. Chem. Soc. 2017, 139, 3456−3464

Phase segregation has been demonstrated in the case of gold NCs capped by a binary ligand shell of octanethiol and mercaptopropionic acid,[25] with different molecules even demonstrating grouping in ripples or Janus-like domains.[26] Interestingly, such patchy or Janus-like ligand shells can help direct NC self-assembly or tune NC properties.[27] Extending these results to colloidal QDs is not straightforward for several reasons. First, QDs are typically made of multicomponent materials, such as CdSe, PbS, InP, or $CuInS_2$.[2] As a result, the QDs are terminated by facets with distinctly different compositions and concomitantly different headgroup−substrate interactions. Second, a delicate interplay exists in such QDs between the surface composition and the ligand surface concentration, where excess surface metal cations are charge balanced by an equivalent of so-called X-type ligands, such as carboxylates or phosphonates.[28,29] This restricts newly added X-type ligands to only replace existing ligands rather than adding to the ligand shell, which is contrasting to gold NCs exposed to thiols, for which both mechanisms are viable.[30]

Here, we report a combined experimental and theoretical study on two-component ligand shells of colloidal QDs made by ligand exchange. Taking oleate-capped CdSe QDs as a model system,[28] we first show by nuclear magnetic resonance (NMR) spectroscopy that exposure to other fatty acids results in a one-for-one exchange that leaves the net ligand/excess cadmium balance unchanged. In the case of saturated primary carboxylic acids, this exposure results in a progressive exchange toward a two-component ligand shell that has the same composition as the reaction mixture. Meanwhile, exposure to a branched carboxylic acid leads only to a partial replacement of the original ligands, regardless of the concentration of the branched acid. Describing the QD surface as a two-dimensional lattice, we attribute this restricted exchange to a combination of a one-for-one exchange reaction and a difference in chain volume. Whereas such a model cannot distinguish a randomly distributed ligand shell from a phase-separated two-component ligand shell, detailed molecular dynamics (MD) simulations support an interpretation where the particular surface chemistry of CdSe QDs results in (100) facets that are densely packed with oleate ligands. As branched acids cannot attain the same surface concentration, ligand exchange is restricted to the sparsely capped facets and facet edges. This indicates that in the case of QDs of binary semiconductors, two-component ligand shells can phase separate due to the differences in facet-specific adsorption, ligand−ligand interaction, and surface concentration imposed by the surface excess of metal cations.

EXPERIMENTAL SECTION

CdSe Quantum Dot Synthesis. CdSe QDs were synthesized according to a procedure developed by Jasieniak et al.[31] In brief, a mixture of cadmium oleate (0.36 mmol), oleic acid (OA, 2.16 mmol), and octadecene (ODE, 12 mL) was stirred under a nitrogen flow for 30 min at 100 °C. The nitrogen flow was stopped, and, still under nitrogen, the temperature was raised to 260 °C. Next, 3.6 mL of a 0.1 M solution of selenium (0.36 mmol) in ODE was injected after which the reaction mixture was kept at a temperature of 235 °C. To purify the CdSe QDs, equal amounts of toluene, 2-propanol, and methanol were added to the reaction in a 1:1 ratio with respect to the volume of ODE. The mixture was centrifuged, and the resulting pellet was redispersed in toluene. This mixture was further purified twice using methanol and toluene as the nonsolvent and the solvent, respectively.

Analysis of Absorption Spectra. UV−vis absorption spectra of purified QD dispersions were recorded for quantitative analysis according to a previously described procedure.[32] In brief, by means of the zb-CdSe sizing curve,[33] the mean QD diameter, d_{NC}, was calculated from the peak wavelength of the first exciton transition. The amount of CdSe formed n_{CdSe} was obtained from the average absorbance of a diluted aliquot at 300, 320, and 340 nm and the intrinsic absorption coefficient of CdSe QDs at these respective wavelengths.[33]

Nuclear Magnetic Resonance Spectroscopy. Samples for NMR studies were prepared by drying a dispersion of CdSe QDs in a nitrogen-filled glovebox using a strong nitrogen flow. The resulting dry QD powder was redispersed in deuterated toluene-d_8 (99.5%D, purchased at Euriso-top) or deuterated 1,2-dichlorobenzene-d_4 (99,5% D, purchased at Euriso-top) and transferred to an NMR tube. High-resolution NMR measurements were recorded on a Bruker Avance III spectrometer operating at a ^{1}H frequency of 500.13 MHz and equipped with a BBI-Z probe or on a Bruker Avance II spectrometer operating at a ^{1}H frequency of 500.13 MHz and equipped with a TXI-Z probe (channels are ^{1}H, ^{13}C, ^{31}P). The sample temperature was set to 298.15, 333.15, 348.15, or 393.15 K. Quantitative ^{1}H spectra were recorded with a 20 s delay between scans to allow full relaxation of all NMR signals. The quantification was done by using the Digital ERETIC method. All resonances were corrected prior to integration by subtracting a background from the measured intensity.

Molecular Dynamics Simulations. Classical MD simulations were carried out on a nonstoichiometric $Cd_{1012}Se_{911}$ QD, carved from a bulk zinc-blende structure. This QD had a size of ∼4 nm and featured four (100), four Cd-rich (111), four Se-rich ($\overline{111}$), and eight (101) staircase facets. In all simulations, we included 202 X-type ligands, which were necessary to fully compensate the excess of positive metal (Cd) charge. L-type ligands were excluded in the simulations as their effect is considered negligible. Both homogeneous and heterogeneous organic ligand shells were investigated, constituted by either oleates or 2-hexyldecanoate, or a mixture of the two. More details on each calculation performed for a given fraction of bound ligands are provided later in the text.

To obtain a meaningful distribution of ligands on the NC surface, we randomly placed the 202 X-type ligands on the surface of a virtual ∼5 nm sphere encompassing the whole NC. In this way, the ligands were positioned at ∼1 nm from the QD surface, with their headgroups loosely pointing toward the surface. We then let the ligands relax on the QD surface by performing a 15 ns MD simulation in vacuum at constant volume and energy and restraining the position of the inorganic core atoms, Cd and Se, with a very stiff harmonic potential (k = 15,000 kJ/mol) to maintain the QD integrity. Afterward, we placed the QD in a cubic box with sides of 11 nm and filled with dichloromethane, which acted as the solvent. This simulation box spans about 70,000 atoms, represented by about 50,000 particles. On this system we performed an initial relaxation by carrying out a complete steepest-descent minimization toward the closest minimum, followed by a 1.5 ns MD simulation at a constant pressure of 1 atm and a temperature of 500 K using a Berendsen barostat and thermostat, respectively.[34] In both passages, the QD atoms and the carboxylate groups of the ligands were restrained in the positions obtained from the minimization step. In a subsequent step, we allowed all atoms to relax by annealing the temperature from 500 to 298 K in 20 ns using a velocity rescaling thermostat and maintaing the pressure at 1 atm with a Parinello−Rahman barostat.[35−37] After the annealing, each system was equlibrated for an additional 20 ns.

The classical force-field potential employed in all calculations was taken by CHARMM. In particular, the interactions between Cd, Se, and O atoms were modeled by using a simple Lennard-Jones potential and a Coulomb interaction between point charges. Parameters for Cd, Se, and carboxylate headgroup atoms were taken from the literature.[38] Dichloromethane was described using a unified-atom model, where the $-CH_2$ group was approximated as a single unit. All simulations were performed using GROMACS.

RESULTS

Carboxylic Acid Exchange Stoichiometry. In this study, we used CdSe QDs synthesized from cadmium oleate and

DOI: 10.1021/jacs.6b11328
J. Am. Chem. Soc. 2017, 139, 3456−3464

elemental selenium in a reaction where OA was the sole ligand; a procedure first described by Jasieniak et al.[31] The method typically yields ~3.5 nm CdSe QDs stabilized by oleates,[28] as attested by the ^{1}H NMR spectrum of a purified dispersion in 1,2-dichlorobenzene-d_4 represented in Figure 1a. Similarly to previously published work,[28] the spectrum features the broadened resonances characteristic of bound oleate, with the unobstructed alkene resonance being observed at ~5.65 ppm. As the spectrum is acquired under quantitative conditions, the integrated intensity of this resonance (indicated by the shaded area in the inset of Figure 1a) is directly proportional to the amount of bound ligands in the dispersion. From this number, we calculate a ligand surface concentration of 3.2 nm^{-2} for the example shown.

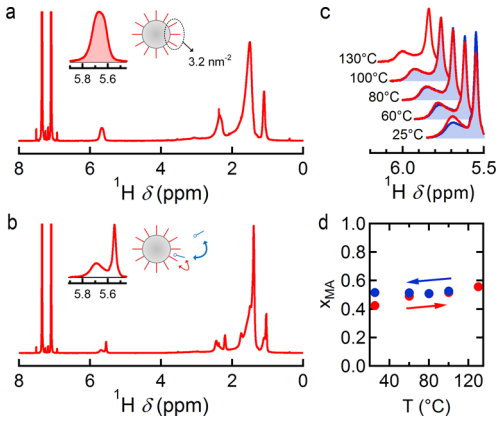

Figure 1. (a) 1D ^{1}H NMR spectrum of oleate-capped CdSe QDs in 1,2-dichlorobenzene-d_4. Inset: Zoom on the resonance of the alkene protons at ~5.65 ppm and a cartoon representation of a NC featuring tightly bound ligands. (b) 1D ^{1}H NMR spectrum of oleate-capped CdSe NCs after addition of 1 equiv of MA in 1,2-dichlorobenzene-d_4. Inset: Zoom on the resonance of the alkene protons and a cartoon representation of the two-step exchange reaction that accounts for the changes in the NMR spectrum.[28] (c) 1D ^{1}H NMR spectra of the alkene resonance after addition of 1 equiv of MA recorded at different temperatures as indicated during a temperature sweep from (red) 25 to 130 °C and (blue) back to 25 °C. (d) The fraction of bound MA as a function of temperature during (red markers) the forward and (blue markers) the backward temperature sweep.

Upon addition of a primary saturated carboxylic acid—myristic acid (MA) in this case—each broadened resonance acquires a second, sharper resonance at its upfield side (see Figure 1b). This is clearly visible in the inset of Figure 1b, which shows a zoom of the alkene region. The additional resonance has been amply discussed in the literature for the case where additional OA was added to oleate-capped CdSe QDs.[28] As shown by the cartoon inset in Figure 1b, it is a population-averaged resonance, assigned to free OA in rapid exchange with OA physisorbed to the CdSe QDs (blue arrow). The bound oleate making up the broad resonance was shown to exchange, albeit slowly, with this pool of free OA (red arrow). On the other hand, the total amount of bound oleate was found to remain constant, regardless of the excess OA concentration.

Figure 1c indicates that an increase in temperature from 25 to 130 °C changes the shape and intensity of both resonances. These changes, however, show no hysteresis when sweeping the temperature from 25 to 130 °C and back to temperatures above 60 °C. We thus conclude that the addition of MA induces the release of OA from the CdSe QDs and establishes a dynamic equilibrium between bound and free ligands for temperatures exceeding ~60 °C. A minor second resonance also develops upon heating a purified dispersion of oleate-capped CdSe QDs (see Supporting Information, Section S1). This observation points toward some thermally induced ligand desorption, where we estimate that ~4% of the originally bound oleate ligands are released at 60 °C.

Carboxylic acids bind to CdSe QDs as carboxylates in a charge-balanced 2:1 ratio with respect to the excess Cd cations on the CdSe surface. Given the need of colloidal QDs dispersed in apolar solvents to preserve charge neutrality,[39] one thus expects the release of OA upon addition of a carboxylic acid to concur with the binding of a carboxylate to the CdSe surface. Writing the core CdSe QD as [CdSe], a carboxylic acid in general as HX, and a surface cadmium carboxylate as (CdX_2), the presumed exchange reaction can then be written as

$$[\mathrm{CdSe}](\mathrm{CdX_2}) + \mathrm{HX'} \rightleftharpoons [\mathrm{CdSe}](\mathrm{CdXX'}) + \mathrm{HX} \qquad (1)$$

Within this picture, the minor release of ligands observed upon heating a purified CdSe QD dispersion can be interpreted as desorption of the entire cadmium oleate moieties or of residual bound carboxylic acid, which can leave as uncharged Z- or L-type ligands, respectively. While the stoichiometry of such exchange reactions has already been verified for the oleate/OA self-exchange[28] and for the replacement of carboxylates by alkyl phosphonates on CdSe QDs,[29] we choose to determine it for a different carboxylic acid. A most interesting choice in this respect is undecenoic acid, because this ligand features alkene resonances that show little overlap with other resonances. We thus titrated as-synthesized oleate-capped CdSe QDs using undecenoic acid to explicitly establish the exchange equilibrium expressed by eq 1 for a carboxylate/carboxylate replacement.

Figure 2a shows four examples of 1D ^{1}H NMR spectra recorded during a titration of oleate-capped CdSe QDs with

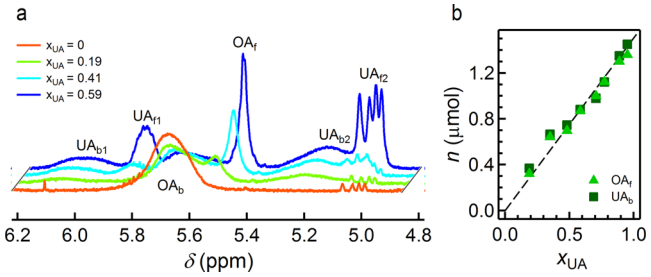

Figure 2. (a) 1D ^{1}H NMR spectra of a dispersion of oleate-capped CdSe QDs after addition of different amounts of undecenoic acid, yielding overall undecenoic mole fractions as indicated. OA and UA indicate resonances pertaining to oleic and undecenoic acid, respectively, whereas the subscripts b and f refer to pools of bound and free ligands. (b) Amount of (light green triangles) free oleate and (dark green squares) bound undecenoate as a function of the overall fraction of undecenoate in the dispersion. The dashed line is a guide to the eye.

undecenoic acid. Starting from the bound-oleate-only spectrum of the as-synthesized QDs, the series of spectra clearly shows a decrease in the intensity of the bound oleate (OA_b) resonance and a concomitant increase of the free oleic acid (OA_f) and bound undecenoate (UA_b) resonances when the overall mole fraction of undecenoic acid is raised. As such, the concentration of all bound and free ligands can be determined from the same,

DOI: 10.1021/jacs.6b11328
J. Am. Chem. Soc. 2017, 139, 3456−3464

quantitative ^{1}H spectrum using the integrated intensity of the respective resonances. Figure 2b represents both the amount of free OA and bound undecenoate—calculated from all spectra recorded during the titration—as a function of the overall fraction of undecenoic acid in the dispersion. In agreement with a recent report by Knauf et al.,[40] we find that both species are present in equal amounts, which confirms the presumed stoichiometry of the carboxylate/carboxylate replacement as expressed by eq 1. In what follows, we will assume that the same exchange reaction applies for any aliphatic primary carboxylic acid added to a dispersion of oleate-capped CdSe QDs.

Oleic Acid/Primary Carboxylic Acid Replacement. Figure 3a shows a zoom on the alkene region of the NMR

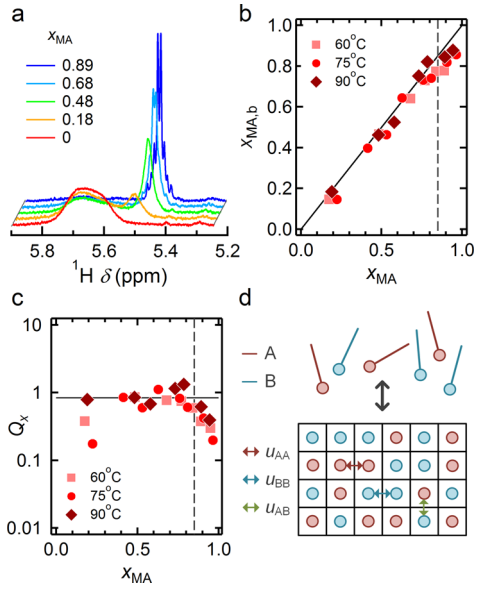

Figure 3. (a) 1D ^{1}H NMR spectra of a dispersion of oleate-capped CdSe QDs after addition of different amounts of MA at 60 °C, yielding overall myristic mole fractions as indicated. (b) The mole fraction of bound myristate, $x_{MA,b}$, in the ligand shell as a function of the overall mole fraction of MA, x_{MA}, in the entire dispersion at 60, 75, and 90 °C (c) The reaction quotient for each step in the titration at 60, 75, and 90 °C as a function of x_{MA}. (d) Lattice model representation of a binary ligand shell containing ligands labeled as A and B, for example, representing bound OA and bound MA.

spectrum of originally oleate-capped CdSe QDs during successive steps of a titration with MA at 60 °C. Upon increasing the overall mole fraction x_{MA} of MA from 0 to 0.89, one sees that the upfield resonance of rapidly exchanging OA gains intensity at the expense of the broad resonance of bound oleate. Concurrently, the alkene resonance of the exchanging OA develops the fine structure typical of unbound OA, indicative of an increasing quantity of free OA in solution. Similar observations are made upon titrating with other primary carboxylic acids—generally written as XA—such as nonanoic acid and undecenoic acid.

Since any release of OA is matched by the equivalent adsorption of myristate, the NMR spectra, as shown in Figure 3a, can be used to determine the composition of the ligand shell. To do so, we use the amount of bound oleate ($n_{OA,b}$) and released OA ($n_{OA,f}$), as determined from the NMR spectra, to calculate the mole fraction, $x_{XA,b}$, of the newly bound carboxylate:

$$x_{XA,b} = \frac{n_{XA,b}}{n_{OA,b} + n_{XA,b}} = \frac{n_{OA,f}}{n_{OA,b} + n_{OA,f}} \quad (2)$$

We note that in this approach the minor self-desorption of oleate or OA moieties from the CdSe QDs is neglected. In Figure 3b, $x_{XA,b}$ is plotted as a function of the overall mole fraction x_{MA} for 3 different temperatures, i.e., 60, 75, and 90 °C. Overall, it follows that $x_{MA,b}$ is almost identical to x_{MA}, meaning that the composition of the ligand shell mimics the overall composition of the dispersion under these conditions. Moreover, no pronounced trend as a function of temperature can be discerned (see Figure 3c). This suggests that the increase of the bound myristate fraction with increasing temperature, as seen in Figure 1d, is not a systematic observation. Possibly, it results from the small self-desorption of ligands upon heating. Only at the highest mole fraction of MA ($x_{MA} > 0.85$) does it appear that the ligand shell is somewhat enriched in oleate as compared to the overall composition of the mixture. We believe that this observation reflects the kinetic limitations to the exchange reaction, which would become evident if oleate ligands exhibited a distribution of adsorption enthalpies with the most strongly bound ligands remaining on the NCs. Titrations with nonanoic and undecenoic acid at 60 °C yielded essentially the same picture (see Supporting Information, Section S2).

For the oleate/carboxylate exchange given by eq 1, the mole fractions of the different bound and free species can be used to calculate a reaction quotient, Q_x, defined as:

$$Q_x = \frac{x_{XA,b} \times x_{OA,f}}{x_{XA,f} \times x_{OA,b}} = \frac{n_{OA,f}^2}{n_{OA,b} \times (n_{MA} - n_{OA,f})} \quad (3)$$

Here, in particular, the second equality enables us to calculate Q_x from the experimental data. Except for two outliers, Figure 3c demonstrates that the determined reaction quotient is largely constant at $Q_x = 0.84$ when $x_{MA} < 0.85$. This result implies that mole fractions can be suitably used as the activities of dissolved carboxylic acids and bound carboxylates. For the former, this is no surprise as the mixture can be considered as ideal-dilute at the given concentrations. In the case of the bound carboxylates, however, it indicates that the capping can be seen as an ideal mixture of two carboxylates, where the activity essentially stems from the entropy of mixing. Using a lattice model representation of a binary ligand shell containing bound OA and bound MA, as shown in Figure 3d, this result suggests that the oleate-myristate nearest-neighbor interaction (indicated us u_{AB} in Figure 3d) equals the average of the oleate−oleate and myristate−myristate nearest-neighbor interactions. Indeed, if such conditions apply, the chemical potential of either of the bound carboxylates can be written as $\mu_{XA,b} = \mu^\circ_{XA,b} + RT \ln x_{XA,b}$, where the standard state refers to the respective one-component ligand shell. Such an expression immediately accounts for the mole fractions of the bound species appearing in the reaction quotient when the exchange reaction is seen as the one-on-one replacement of bound oleate by bound myristate:

$$OA_b + MA_f \rightleftharpoons MA_b + OA_f \quad (4)$$

Interpreting the average value of Q_x as the equilibrium constant of the exchange reaction (eq 1), we obtain a standard exchange free energy $\Delta_{ex}G^\circ$ of only about 0.5 kJ mol^{-1} at 60 °C. Moreover, since the average of Q_x shows little temperature dependence, the exchange enthalpy should be negligible. This

DOI: 10.1021/jacs.6b11328
J. Am. Chem. Soc. 2017, 139, 3456−3464

implies that the exchange reaction expressed by eq 1 involves no net change in ligand−solvent and ligand−ligand interaction energy. Moreover, it means that $\Delta_{ex}G^{\circ}$ nearly vanishes due to a negligible exchange enthalpy and exchange entropy. The composition of the ligand shell will therefore match the overall mole fraction of both carboxylic acids in the dispersion to maximize the entropy of mixing, which is the remaining driving force for the exchange reaction.

Oleic Acid/Branched Carboxylic Acid Replacement. Since two-component ligand shells consisting of oleate and a second primary carboxylate behave as almost ideal mixtures, we extended this study to titrations of as-synthesized oleate-capped CdSe QDs with 2-hexyldecanoic acid (2-HDA). This is a commercially available branched carboxylic acid (see Figure 4a), such that steric hindrance may affect its distribution within

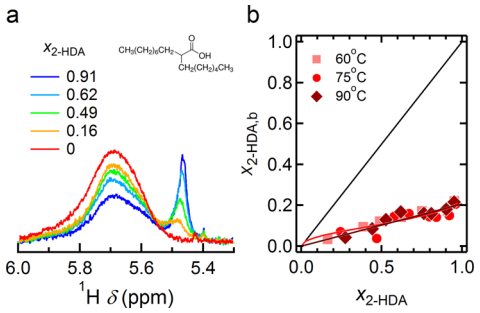

Figure 4. (a) 1D ^{1}H NMR spectra of a dispersion of oleate-capped CdSe QDs after addition of different amounts of 2-HDA at 60 °C, yielding overall 2-hexyldecanoic mole fractions as indicated. (b) Fraction of bound 2-hexyldecanoate $x_{2\text{-HDA,b}}$ as a function of the overall molar fraction of 2-HDA $x_{2\text{-HDA}}$ in the dispersion at 60, 75, and 90 °C. Best fits of the experimental data to (dark red) a straight line and (red) eq 6 are added.

the ligand shell. Upon addition of 2-HDA, the development of a relatively sharp resonance, upfield-shifted relative to the alkene resonance of bound oleate again attests the exchange between OA and 2-HDA according to eq 1. However, in this case, a considerable fraction of the oleate ligands remain bound to the surface, even if the overall mole fraction of 2-HDA is raised to 0.95. More precisely, Figure 4b indicates that the mole fraction of bound 2-HDA in the ligand shell levels off at $x_{2\text{-HDA,b}} \approx 0.2$. This is in strong contrast to what was found for primary carboxylic acids.

Given the one-for-one exchange between carboxylic acids (eq 1), the exchange of a primary for a branched carboxylic acid will raise the volume occupied by the alkyl chains in the ligand shells. In this respect, steric hindrance may restrict the amount of 2-HDA that can be accommodated in the ligand shell. Indeed, a straightforward calculation that assumes a ligand molar volume characteristic of OA indicates that the volume of the bound ligands can amount to 50−70% of the volume available in the ligand shell for 3.5 nm spheres with a ligand surface concentration, σ, of 3−4 nm^{-2} (see Figure 5a). Hence, it is well possible that the limited accessible volume in the ligand shell imposes an upper limit on the OA/2-HDA exchange.

Different approaches can be put forward to account for the remaining free volume in the ligand shell within a lattice model description of the QD surface. First, the surface of the original, oleate-capped QDs can be described as a random mixture of lattice sites occupied by oleate ligands and unoccupied sites

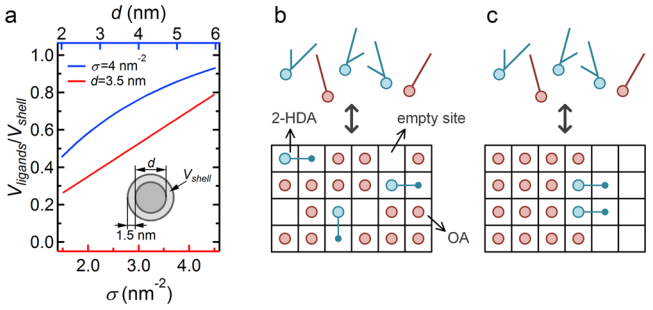

Figure 5. (a) Fraction of the ligand shell volume occupied by OA ligands plotted as a function of (blue) the NC diameter at a fixed ligand surface concentration σ = 4 nm^{-2} and (red) the surface concentration for d = 3.5 nm NCs. All calculations assume spherical NCs featuring a 1.5 nm thick, concentric ligand shell. (b) Lattice model representation of a ligand shell consisting of a random mixture of free lattice sites and sites occupied by (red) bound OA and (blue) bound 2-HDA. (c) Lattice model representation of a ligand shell consisting of domains of densely packed bound OA and ligand-free domains, where 2-HDA exchange is restricted to domain edges.

(see Figure 5b), the latter reflecting the remaining available space in the ligand shell. Whereas the exchange of oleate for a primary carboxylate will leave the number of unoccupied sites unchanged, this number will decrease when an oleate ligand is replaced by a branched carboxylate like 2-HDA. Assuming that bound 2-HDA occupies two lattice sites, we can then rewrite the OA/2-HDA exchange as a reaction in which bound OA and a free site (denoted as ◯) are exchanged for bound 2-HDA:

$$\mathrm{OA_b} + 2 - \mathrm{HDA_f} + \bigcirc \rightleftharpoons 2 - \mathrm{HDA_b} + \mathrm{OA_f} \qquad (5)$$

Using volume fractions for activities of bound ligands, the exchange equilibrium expressed by eq 5 can be turned into a relation between the mole fractions of bound and total 2-HDA (see Supporting Information, Section S3):

$$x_{2\text{-HDA,b}} = \frac{\sqrt{(K' x_{2\text{-HDA}})^2 + 8\Delta K' x_{2\text{-HDA}}(1 - x_{2\text{-HDA}})} - K' x_{2\text{-HDA}}}{4(1 - x_{2\text{-HDA}})} \qquad (6)$$

where K' is a constant, closely related to the equilibrium constant of the exchange reaction and Δ is the ratio between originally empty and occupied lattice sites. A fit of the experimental data to eq 6 has been added to Figure 4b, where K' and Δ have been used as adjustable parameters. As anticipated, the lattice model predicts an incomplete exchange in the limit $x_{2\text{-HDA}} \rightarrow 1$, where a best fit is obtained with Δ = 0.22. Hence, about 20% of the lattice sites would be initially unoccupied. The estimates summarized in Figure 5a, however, indicate that 50% of the ligand shell volume should be available at a ligand surface concentration of 3.0 nm^{-2} for a 3.5 nm QD. As this implies that full coverage by 2-HDA should still be possible, a limiting value of $x_{2\text{-HDA,b}} \approx 0.2$ seems rather low.

An alternative interpretation of the restricted OA/2-HDA exchange starts from the idea that the typical surface concentration of 3.0−3.5 nm^{-2} reflects an average across all NC facets, with each featuring a different surface concentration. Looking at cadmium oleate as the actual binding moiety, this is not an unreasonable conjecture given the facet-dependent coordination number of surface selenium atoms. The (100) surface, for example, features two-coordinated surface selenium atoms that offer two bonds for each cadmium oleate ligand, while the Se($\overline{111}$) surface is composed of three-coordinated

DOI: 10.1021/jacs.6b11328
J. Am. Chem. Soc. 2017, 139, 3456−3464

surface selenium atoms to which cadmium oleate can be expected to bind more weakly. In this picture, the combination of steric hindrance on the densely packed facets and weak binding to the free facets may limit the OA/2-HDA exchange to the edges of the densely packed facets (see Figure 5c). Assuming ideal mixing at these accessible surface sites, $x_{2\text{-HDA,b}}$ will then increase proportionally with $x_{2\text{-HDA}}$, where the limiting value at $x_{2\text{-HDA}} = 1$ reflects the fraction of accessible sites. Clearly, the experimental data set does not enable us to distinguish between such a linear dependence of $x_{2\text{-HDA,b}}$ on $x_{2\text{-HDA}}$ and the more involved variation predicted by eq 6.

Molecular Dynamics Simulations of Two-Component Ligand Shells. To test the above hypotheses, we carried out MD simulations on two-component ligand shells with different fractions of bound oleate and 2-hexyldecanoate. For this purpose, we carved a nonstoichiometric $Cd_{1012}Se_{911}$ NC of about 4.0 nm in diameter (Figure 6a) out of a bulk zinc blende

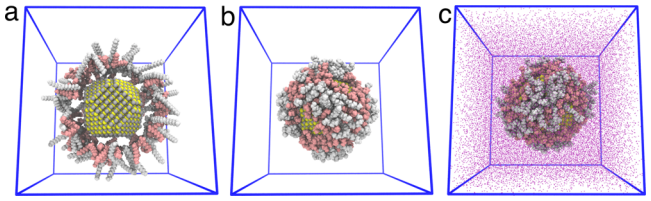

Figure 6. Stepwise procedure to simulate homogenoues and heterogeneous ligand shells of a ~4.0 nm $Cd_{1012}Se_{911}$ QD for the example of a $x_{2\text{-HDA}} = 0.5$ ligand shell. Oleate is represented in white and 2-hexyldecanoate in pink. (a) Initial random placement of 202 X-type carboxylate ligands at ~1 nm from the QD surface. (b) Ligands are relaxed onto the QD surface in vacuum for 15 ns, at constant volume and energy. Velocities are initialized at 500 K and the positions of Cd and Se are restrained. (c) Both the NC and the ligands are free to move in a simulation box with 11 nm sides and filled with dichloromethane. Temperature is annealed from 500 to 298 K for 20 ns in an isothermic-isobaric ensemble at 1 atm.

crystal. To preserve charge neutrality of the system, we distributed 202 carboxylate ligands on the QD surface yielding an average ligand surface concentration of 3.43 nm^{-2}. This ligand surface concentration is in close agreement with the experimental figure for the oleate-capped CdSe QDs used here. It should be clear, however, that all quantitative calculations on ligand surface concentrations will yield somewhat different numbers when the simulations are run using a CdSe NC with a slightly different Cd:Se ratio. Different ligand shell compositions were studied with $x_{2\text{-HDA}}$ ranging from 0.00 to 0.25, 0.50, 0.75, and 1.00. Here, the range extremes were homogeneous shells of OA and 2-HDA, respectively, and the intermediate ones had two-component shells.

For each ligand shell composition, we performed stepwise MD simulations, where ligands were allowed to find their most suitable position on the QD surface. As shown in Figure 6, this procedure consisted of three successive steps: (1) carboxylate ligands with a given oleate fraction being randomly placed at some fixed distance from the surface; (2) the ligands were allowed to move to the QD surface, while all Cd and Se atoms were restrained to a fixed position; and (3) the whole system, including the inorganic core, was relaxed in a simulation box that included the ligand-capped NC and solvent. We used dichloromethane as the solvent since it resembles the solvent that was actually used in the experiments in terms of physicochemical properties, while allowing for a coarse-grained treatment of the solvent in the MD simulations—a substantial computational advantage. After these equilibration steps, we then performed a production run of 20 ns at constant pressure (1 atm) and temperature (298 K) to analyze kinetic and thermodynamic contributions to the distribution of ligands across the QD surface.

Figure 7a represents snapshots of NCs with three different ligand shell compositions, spanning the two homogeneous OA

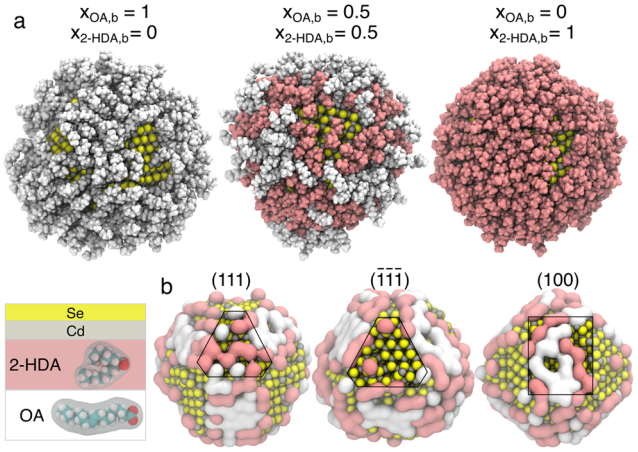

Figure 7. Equilibrated configurations of CdSe QDs with different ligand shells obtained from the MD simulations. (a) Last frame of the simulations for $x_{2\text{-HDA}} = 0$ (pure OA shell), 0.5 (same amount of OA and 2-HDA), and 1 (pure 2-HDA shell) obtained at room temperature. The more patchy surface coverage of a pure OA shell and the more homogeneous coverage of a pure 2-HDA shell are clearly visible. (b) Alternative representation of the final frame for $x_{2\text{-HDA}} = 0.5$ in which only carboxylate groups of ligands are represented, and the QD is oriented so as to give a view on different facets. Accumulation of OA on the (100) facet can be noticed.

and 2-HDA shells and a two-component ligand shell with $x_{2\text{-HDA}} = 0.5$. The eye-catching feature is that even in the pure 2-HDA case, the NC surface can accommodate all 202 ligands. This indicates that steric hindrance, as such, is not the factor limiting the 2-HDA/OA exchange. Even so, the simulated pure OA and pure 2-HDA ligands shells show considerable differences. Most notably, we find that a pure OA shell is more densely packed on the (100) facets (see Table 1). A pure

Table 1. Simulated Ligand Surface Concentrations on the Different Facets of the $Cd_{1012}Se_{911}$ Model QD Covered with OA or 2-HDA Only[a]

system	(100)	(110)	(111)	($\bar{1}\bar{1}\bar{1}$)
$x_{OA} = 1$	4.8	1.3	3.4	0.3
$x_{2\text{-HDA}} = 1$	4.1	3.5	3.8	1.4

[a]Surface concentrations given in nm^{-2}.

2-HDA shell, on the other hand, has a reduced ligand concentration on this facet, which is compensated by a more dense packing on all other facets. Since both ligands are primary carboxylic acids, this more homogeneous spreading of 2-HDA does not reflect different adsorption energies, yet it is probably due to its bulky, branched alkyl chain, which lowers the maximum surface concentration that 2-HDA can attain on a specific facet. In this respect, the increased binding of ligands to the Se-rich ($\bar{1}\bar{1}\bar{1}$) facet stands out, as it is mostly unoccupied in

DOI: 10.1021/jacs.6b11328
J. Am. Chem. Soc. 2017, 139, 3456−3464

the case of a pure OA shell due to the less favorable adsorption of cadmium carboxylates on this facet. Inspection of our MD trajectories reveals that the ligand density build-up on the $(\overline{1}11)$ facets is likely driven by a combination of two phenomena: (i) the displacement of some of the edge Cd-carboxylate (Z-type) groups that diffuse toward the available Se atoms in the $(\overline{1}11)$; and (ii) the diffusion of subshell Cd atoms toward the $(\overline{1}11)$ surface and the consequent passivation of these Cd atoms with 2-HDA ligands diffusing from the edge sites.

In Figure 7b, we look more closely at these different facets in the case of the two-component ligand shell with $x_{2\text{-HDA}} = 0.5$. The color coding with OA in white and 2-HDA in pink readily indicates that the ligands tend to arrange in three specific subdomains: (1) densely packed and almost pure domains of oleate ligands on (100) facets; (2) mixed composition subdomains at the Cd-rich (111) facets; and (3) 2-HDA passivated Se-rich $(\overline{1}11)$ facets, as well as edges between facets. We verified the effect of temperature on the formation of these subdomains by carrying out one additional 100 ns long MD simulation for $x_{2\text{-HDA}} = 0.5$ at constant temperature and pressure, 500 K and 1 atm, respectively. The final distribution of ligands is consistent with the ones obtained at room temperature. This agrees with the experimental findings, although a narrower temperature range is addressed there, and indicates that the appearance of separate subdomains is not the result of kinetic restrictions in the MD simulations. Instead it represents a thermodynamically stable state of the ligand shell at both low and high temperatures.

To quantify the impression that OA ligands are enriched on the (100) facets, we focused on the radial distribution of ligands around a given central ligand. To do so, two neighboring ligands are characterized by the distance between the carbon atoms of the anchoring carboxylate groups. The inset of Figure 8a represents the radial distribution function obtained for a pure OA shell. It features an initial maximum at a radial distance r of around 0.47 nm, followed by a minimum at 0.65 nm. These numbers can be interpreted as the average distance between nearest-neighbor ligands and the radius where the first coordination ring ends, respectively. In what follows, we will therefore use the average number, $n_{XA/X'A}$, of X′A ligands around an XA ligand at a radial distance r of 0.65 nm to characterize the average local environment of XA ligands (see Figure 8d). Figure 8a represents $n_{OA/OA}$ and $n_{2\text{-HDA/2-HDA}}$ as a function of r for the case of a pure OA and a pure 2-HDA ligand shell, respectively. The figure shows, for example, that on average, 3.9 OA ligands can be found within a distance of 0.65 nm around a given OA ligand in a pure OA ligand shell, whereas in the case of a pure 2-HDA shell, the corresponding number drops to 2.9 2-HDA ligands. Clearly, these numbers attest the preferential grouping of OA on the densely packed (100) facet, which is in contrast with the more uniform distribution of 2-HDA over all facets.

In the case of a random distribution of equally sized objects, $n_{OA/OA}$ and $n_{2\text{-HDA/2-HDA}}$ will be simply proportional to the molar fraction of OA and 2-HDA in the ligand shell, respectively. As shown in Figure 8b, this is indeed the case for 2-HDA. This agrees with our initial conclusion that 2-HDA is mainly found on facets with a mixed composition. On the other hand, it appears that $n_{OA/OA}$ is systematically larger than expected, which confirms the tendency of OA ligands to bunch, as already inferred from the snapshots shown in Figure 7b. Importantly, the numbers shown in Figure 8b are averages taken over all NC facets. Restricting the analysis to ligands

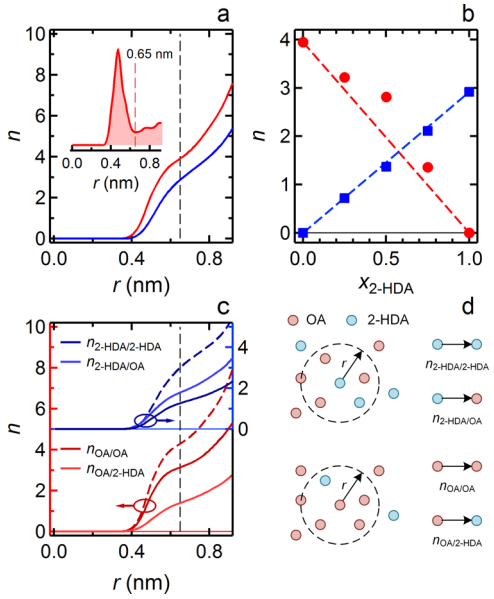

Figure 8. (a) Average number $n(r)$ of (red) OA ligands around a given OA ligand and (blue) 2-HDA ligands around a given 2-HDA ligand for different ligand shell compositions as a function of the distance r from the central ligand. The dashed line indicates the distance $r = 0.65$ nm that characterizes the end of the first coordination ring. Inset: Radial distribution function obtained for a pure OA ligand shell. (b) Variation of $n(r)$ at $r = 0.65$ nm as a function of the ligand shell composition for OA/OA and 2-HDA/2-HDA combinations. The dashed lines give the linear variations of the ligand number with x_{OA} as a reference. (c) Average number of (red curves) OA and 2-HDA ligands around an average OA ligand on the (100) facet and (blue curves) OA and 2-HDA ligands around an average 2-HDA ligand. The dashed lines give $n_{OA/OA}$ and $n_{2\text{-HDA/2-HDA}}$ for pure OA and 2-HDA ligand shells as a reference. (d) Cartoon representation of the ligand numbers around an average (top) 2-HDA and (bottom) OA ligand on the (100) surface. In both cases, the ligands are distributed so as to highlight the OA enrichment of the local environment.

found on (100) facets in the case of a two-component ligand shell with $x_{2\text{-HDA}} = 0.5$ corroborates this conclusion. Focusing first on the OA ligands (see Figure 8c, bottom), we find that $n_{OA/OA}$ is always larger than $n_{OA/2\text{-HDA}}$, meaning that an average OA ligand on the (100) facet is preferentially surrounded by other OA ligands (see Figure 8d, bottom). Taking again $r = 0.65$ nm, Table 2 indicates that the ratio $n_{OA/OA}/n_{OA/2\text{-HDA}}$ amounts to 2.25. Similarly, $n_{2\text{-HDA/OA}}$ exceeds $n_{2\text{-HDA/2-HDA}}$, indicating that an average 2-HDA ligand on the (100) facet features a local environment enriched in OA as well.

From our simulations, we can conclude that the incomplete ligand exchange of the native oleates with the branched 2-HDA ligands is linked to a restricted ligand mixing at the NC surface. In the case of a pure OA capping, ligands tend to bunch on the (100) facet where binding is favorable and a high surface concentration can be achieved thanks to the single aliphatic chain of OA. A neat 2-HDA ligand shell cannot maintain this preferred ligand packing due to its bulkier ligand chain, which makes a full ligand exchange also exhibit a net transfer of cadmium carboxylates from the (100) facet to crystal facets less favorable for binding. As a result, ligand exchange is restricted to facet edges and facets with a lower original surface concentration, such as Cd(111). Ligand exchange will stop once these accessible sites are saturated with 2-HDA.

DOI: 10.1021/jacs.6b11328
J. Am. Chem. Soc. 2017, 139, 3456−3464

Table 2. Simulated Ligand Numbers within a Distance r = 0.65 nm[a] around a Given Ligand on the (100) Facet for the Ligand Compositions as Indicated

$x_{2\text{-HDA}}$	0	0.5				1
pair	OA/OA	OA/OA	OA/2-HDA	2-HDA/OA	2-HDA/2-HDA	2-HDA/2-HDA
n	4.32	3.16	1.41	1.81	1.28	3.06

[a]See vertical dashed line in Figure 8c.

DISCUSSION

Branched carboxylic acids, such as 2-HDA, have raised interest recently as so-called entropic ligands that can enhance the solubility of QDs in liquid or solid sols.[41] However, the ligand exchange results shown here indicate that straight-chain and branched carboxylic acids ligands are not merely equivalent ligands. Whereas the original oleate ligands of CdSe NCs can be largely replaced by any straight-chain carboxylate, their exchange for 2-hexyldecanoate is limited to 20−25%. According to MD simulations, this is mainly due to the dense packing of straight-chain carboxylates on the (100) surface, which suggests that the experimental ligand surface concentration of 3.0−3.5 nm^{-2} should be seen as a facet-area weighted average of high-density facets, such as (100), and almost bare facets, such as Se($\overline{111}$). This particular ligand distribution, which should come with a concomitant facet-specific distribution of excess cadmium, can be preserved when the original oleate ligands are replaced by straight-chain carboxylates. On the other hand, this factor prohibits the complete exchange of oleate for 2-HDA and, thus, makes postsynthesis ligand exchange inadequate for the formation of QDs with a complete branched ligand capping.

An obvious alternative to form NCs with a complete branched ligand capping is to exclusively use the desired branched carboxylic acid during synthesis. The MD simulations indicate that this can indeed lead to NCs featuring similar, facet-averaged ligand surface concentrations as obtained when using straight-chain ligands. On the other hand, the simulations show that a such a neat capping of branched ligands involves a different distribution of ligands—best seen as cadmium carboxylates at this point—over the NC facets, with less populated (100) facets and more populated Cd(111) and Se($\overline{111}$) facets. Interestingly, comparing CdSe NCs synthesized using straight chain acids and dialkyl acids, such as 2-hexadecanoic and 2-butyloctanoic acid, Morris et al. reported that the use of branched acids strongly enhances trap-related emission.[42] On the other hand, it was shown by Anderson et al. that the progressive displacement of cadmium oleate from its original surface sites results in an abrupt quenching of the photoluminescence.[20] Hence, the specific organization of branched carboxylates over the CdSe surface, involving a reduced surface concentration on the (100) surface, may indeed translate into a poorer optical performance of CdSe NCs synthesized using branched carboxylic acids.

CONCLUSIONS

We have monitored ligand exchange reactions on CdSe QDs using solution NMR spectroscopy where originally present oleate (OA) ligands were replaced by single-chain or branched primary carboxylic acids. In both cases, a binary ligand shell was formed. However, while the ligand shell composition mostly matched the carboxylic acid composition of the entire dispersion for single-chained acids, only 20−25% of the oleate ligands could be replaced by the branched carboxylate 2-hexadecanoate (2-HDA). Through classical MD simulations, we showed that this restricted ligand exchange is not due to mere volume restrictions in the ligand shell arising from steric interactions, which would inhibit further binding of the bulkier 2-HDA. Instead, the MD simulations suggested that this arises due to facet-specific variations in binding of different ligands. As a specific example, OA preferentially packs on the (100) facet at a higher surface concentration than the bulkier 2-HDA. As a result, we argue that 2-HDA can only replace OA ligands on sparsely capped facets and facet edges, which implies that only a fraction of the OA ligands are available for exchange.

Capping colloidal NCs using branched ligands have been put forward as a way to suppress NC aggregation and, thus, enhance the solid loading in NC dispersions. On the other hand, the proper passivation of NC facets with ligands is key to avoid surface trapping of photoexcited charge carriers and promote radiative recombination. In this respect, the reduced maximum packing density of branched ligands and of concomitant excess metal cations on specific facets may be troublesome, even at comparable average surface concentrations. This makes the use of branched ligands a delicate balancing act, where dispersion stability is traded for electronic passivation.

ASSOCIATED CONTENT

Supporting Information

The Supporting Information is available free of charge on the ACS Publications website at DOI: 10.1021/jacs.6b11328.

Data on titrations of oleate-capped CdSe with undecenoic and nonanoic acid and derivation of eq 6 used to fit the experimental data on oleate for 2-hexyldecanoate exchange (PDF)

AUTHOR INFORMATION

Corresponding Author

*zeger.hens@ugent.be

ORCID

Ivan Infante: 0000-0003-3467-9376

Zeger Hens: 0000-0002-7041-3375

Notes

The authors declare no competing financial interest.

ACKNOWLEDGMENTS

Z.H. acknowledges support by the European Comission via the Marie-Sklodowska Curie action Phonsi (H2020-MSCA-ITN-642656), the Belgian Science Policy Office (IAP 7.35, photonics@be) and BOF-UGent (GOA no. 01G01513). I.I. would like to thank The Netherlands Organization of Scientific Research (NWO) for providing financial support within the Innovational Research Incentive (Vidi) Scheme. DFT calculations were carried out on the Dutch national e-infrastructure with the support of SURF Cooperative. J.J. would like to thank the Australian Research Council through CE170100026.

DOI: 10.1021/jacs.6b11328
J. Am. Chem. Soc. 2017, 139, 3456−3464

REFERENCES

(1) Yin, Y.; Alivisatos, A. P. *Nature* **2005**, *437*, 664−670.
(2) Kovalenko, M. V.; Manna, L.; Cabot, A.; Hens, Z.; Talapin, D. V.; Kagan, C. R.; Klimov, V. I.; Rogach, A. L.; Reiss, P.; Milliron, D. J.; Guyot-Sionnnest, P.; Konstantatos, G.; Parak, W. J.; Hyeon, T.; Korgel, B. A.; Murray, C. B.; Heiss, W. *ACS Nano* **2015**, *9*, 1012−1057.
(3) Abe, S.; Capek, R. K.; De Geyter, B.; Hens, Z. *ACS Nano* **2013**, *7*, 943−949.
(4) De Nolf, K.; Capek, R. K.; Abe, S.; Sluydts, M.; Jang, Y.; Martins, J. C.; Cottenier, S.; Lifshitz, E.; Hens, Z. *J. Am. Chem. Soc.* **2015**, *137*, 2495−2505.
(5) Peng, X. G.; Manna, L.; Yang, W. D.; Wickham, J.; Scher, E.; Kadavanich, A.; Alivisatos, A. P. *Nature* **2000**, *404*, 59−61.
(6) Carbone, L.; Nobile, C.; De Giorgi, M.; Sala, F. D.; Morello, G.; Pompa, P.; Hytch, M.; Snoeck, E.; Fiore, A.; Franchini, I. R.; Nadasan, M.; Silvestre, A. F.; Chiodo, L.; Kudera, S.; Cingolani, R.; Krahne, R.; Manna, L. *Nano Lett.* **2007**, *7*, 2942−2950.
(7) Brust, M.; Walker, M.; Bethell, D.; Schiffrin, D. J.; Whyman, R. *J. Chem. Soc., Chem. Commun.* **1994**, *0*, 801−802.
(8) Kim, T.-H.; Cho, K.-S.; Lee, E. K.; Lee, S. J.; Chae, J.; Kim, J. W.; Kim, D. H.; Kwon, J.-Y.; Amaratunga, G.; Lee, S. Y.; Choi, B. L.; Kuk, Y.; Kim, J. M.; Kim, K. *Nat. Photonics* **2011**, *5*, 176−182.
(9) Carey, G. H.; Abdelhady, A. L.; Ning, Z.; Thon, S. M.; Bakr, O. M.; Sargent, E. H. *Chem. Rev.* **2015**, *115*, 12732−12763.
(10) Keuleyan, S.; Lhuillier, E.; Brajuskovic, V.; Guyot-Sionnest, P. *Nat. Photonics* **2011**, *5*, 489−493.
(11) Saha, K.; Agasti, S. S.; Kim, C.; Li, X.; Rotello, V. M. *Chem. Rev.* **2012**, *112*, 2739−2779.
(12) De Roo, J.; van Driessche, I.; Martins, J. C.; Hens, Z. *Nat. Mater.* **2016**, *15*, 517−522.
(13) Lee, J.-S.; Kovalenko, M. V.; Huang, J.; Chung, D. S.; Talapin, D. V. *Nat. Nanotechnol.* **2011**, *6*, 348−352.
(14) Brown, P. R.; Kim, D.; Lunt, R. R.; Zhao, N.; Bawendi, M. G.; Grossman, J. C.; Bulovic, V. *ACS Nano* **2014**, *8*, 5863−5872.
(15) Stinner, F. S.; Lai, Y.; Straus, D. B.; Diroll, B. T.; Kim, D. K.; Murray, C. B.; Kagan, C. R. *Nano Lett.* **2015**, *15*, 7155−7160.
(16) Lhuillier, E.; Scarafagio, M.; Hease, P.; Nadal, B.; Aubin, H.; Xu, X. Z.; Lequeux, N.; Patriarche, G.; Ithurria, S.; Dubertret, B. *Nano Lett.* **2016**, *16*, 1282−1286.
(17) Chuang, C.-H. M.; Brown, P. R.; Bulovic, V.; Bawendi, M. G. *Nat. Mater.* **2014**, *13*, 796−801.
(18) Jasieniak, J.; Mulvaney, P. *J. Am. Chem. Soc.* **2007**, *129*, 2841−2848.
(19) Hassinen, A.; Moreels, I.; De Nolf, K.; Smet, P. F.; Martins, J. C.; Hens, Z. *J. Am. Chem. Soc.* **2012**, *134*, 20705−20712.
(20) Anderson, N. C.; Hendricks, M. P.; Choi, J. J.; Owen, J. S. *J. Am. Chem. Soc.* **2013**, *135*, 18536−18548.
(21) Templeton, A. C.; Wuelfing, M. P.; Murray, R. W. *Acc. Chem. Res.* **2000**, *33*, 27−36.
(22) Schreiber, F. *Prog. Surf. Sci.* **2000**, *65*, 151−256.
(23) Buergi, T. *Nanoscale* **2015**, *7*, 15553−15567.
(24) Stranick, S. J.; Parikh, A. N.; Tao, Y. T.; Allara, D. L.; Weiss, P. S. *J. Phys. Chem.* **1994**, *98*, 7636−7646.
(25) Jackson, A. M.; Myerson, J. W.; Stellacci, F. *Nat. Mater.* **2004**, *3*, 330−336.
(26) Ong, Q. K.; Reguera, J.; Silva, P. J.; Moglianetti, M.; Harkness, K.; Longobardi, M.; Mali, K. S.; Renner, C.; De Feyter, S.; Stellacci, F. *ACS Nano* **2013**, *7*, 8529−8539.
(27) Vilain, C.; Goettmann, F.; Moores, A.; le Floch, P.; Sanchez, C. *J. Mater. Chem.* **2007**, *17*, 3509−3514.
(28) Fritzinger, B.; Capek, R. K.; Lambert, K.; Martins, J. C.; Hens, Z. *J. Am. Chem. Soc.* **2010**, *132*, 10195−10201.
(29) Gomes, R.; Hassinen, A.; Szczygiel, A.; Zhao, Q.; Vantomme, A.; Martins, J. C.; Hens, Z. *J. Phys. Chem. Lett.* **2011**, *2*, 145−152.
(30) Smith, A. M.; Marbella, L. E.; Johnston, K. A.; Hartmann, M. J.; Crawford, S. E.; Kozycz, L. M.; Seferos, D. S.; Millstone, J. E. *Anal. Chem.* **2015**, *87*, 2771−2778.
(31) Jasieniak, J.; Bullen, C.; van Embden, J.; Mulvaney, P. *J. Phys. Chem. B* **2005**, *109*, 20665−20668.
(32) Abe, S.; Capek, R. K.; De Geyter, B.; Hens, Z. *ACS Nano* **2012**, *6*, 42−53.
(33) Capek, R. K.; Moreels, I.; Lambert, K.; De Muynck, D.; Zhao, Q.; Vantomme, A.; Vanhaecke, F.; Hens, Z. *J. Phys. Chem. C* **2010**, *114*, 6371−6376.
(34) Berendsen, H. J. C.; Postma, J. P. M.; van Gunsteren, W. F.; DiNola, A.; Haak, J. R. *J. Chem. Phys.* **1984**, *81*, 3684.
(35) Parrinello, M.; Rahman, A. *Phys. Rev. Lett.* **1980**, *45*, 1196−1199.
(36) Parrinello, M. *J. Appl. Phys.* **1981**, *52*, 7182.
(37) Parrinello, M. *J. Chem. Phys.* **1982**, *76*, 2662.
(38) Cosseddu, S.; Infante, I. *J. Chem. Theory Comput.* **2017**, *13*, 297−308.
(39) Cirillo, M.; Strubbe, F.; Neyts, K.; Hens, Z. *ACS Nano* **2011**, *5*, 1345−1352.
(40) Knauf, R. R.; Lennox, J. C.; Dempsey, J. L. *Chem. Mater.* **2016**, *28*, 4762−4770.
(41) Yang, Y.; Qin, H.; Jiang, M.; Lin, L.; Fu, T.; Dai, X.; Zhang, Z.; Niu, Y.; Cao, H.; Jin, Y.; Zhao, F.; Peng, X. *Nano Lett.* **2016**, *16*, 2133−2138.
(42) Morris, T.; Zubkov, T. *Colloids Surf., A* **2014**, *443*, 439−449.

DOI: 10.1021/jacs.6b11328
J. Am. Chem. Soc. 2017, 139, 3456−3464